Results in Engineering 29 (2026) 108475

Contents lists available at ScienceDirect

Results in Engineering

journal homepage: www.sciencedirect.com/journal/results-in-engineering

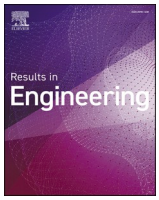

Research paper

The mechanisms of oxide dissolution evolution and mechanical properties transient liquid phase bonding of SSM 6063 aluminum alloy with zamak 2 binder

D. Maunkhaw [a], Y. Dunyakul [a], C. Meengam [b,*]

[a] Faculty of Engineering, Rajamangala University of Technology Srivijaya, Songkhla, 90000, Thailand
[b] Faculty of Industrial Technology, Songkhla Rajabhat University, Songkhla, 90000, Thailand

ARTICLE INFO

Keywords:
Transient liquid phase bonding
SSM 6063 aluminum alloy
Oxide dissolution
Zamak 2
Microstructural analysis
Mechanical properties

ABSTRACT

This study investigates the mechanisms underlying oxide layer evolution and its influence on joint strength during transient liquid phase bonding (TLPB) of SSM 6063 aluminum alloy utilizing Zamak 2 as a binder. The persistent presence of residual oxides in aluminum bonding significantly impedes diffusion kinetics and compromises joint integrity, thereby necessitating a comprehensive investigation into oxide dissolution behavior. This research addresses this gap by systematically evaluating oxide characteristics under varying bonding temperatures (450, 500, and 550 °C) and bonding times (60 and 120 min), under constant bonding pressure and inert gas conditions. A full factorial design of experiments was implemented, and high-resolution microstructural analysis using SEM-EDS was employed to evaluate oxide distribution and interfacial diffusion. The optimal mechanical strength (23.56 MPa) was obtained at 450 °C and 120 min, while oxide formation was minimized. ANOVA revealed that bonding temperature was the most significant factor, followed by bonding time. The regression model explained 89.26 % of the total variation. Defects including cracks, porosity, interfacial separation, and oxide barriers were observed and found to significantly impact joint reliability.

1. Introduction

Transient Liquid Phase Bonding (TLPB) has emerged as a reliable technique for joining aluminum alloys due to its ability to produce strong and defect-free joints [1]. However, the presence of a residual oxide layer on aluminum alloys remains a significant challenge, hindering effective diffusion and limiting the mechanical strength of bonded joints [2]. The oxidation of aluminum alloys, particularly SSM 6063, introduces barriers to metallurgical bonding, necessitating a deeper understanding of oxide evolution and dissolution mechanisms [3]. The role of Zamak 2 as a binder material presents a novel approach to enhancing bonding strength, yet its effectiveness in mitigating oxide-related challenges remains underexplored. For example, at 500 °C, the formation of Ni_3Sn_2 and Ni_3Sn was predominantly governed by volume diffusion as the main growth mechanism and oxide layers frequently inhibit the mechanisms responsible for grain growth [4]. Addressing these issues is crucial for optimizing TLPB processes for high-performance structural applications in aerospace, automotive, and manufacturing industries [5]. Several studies have investigated the effects of oxide layers on aluminum bonding and Zamak 2 interlayer is not a passive "binder" but an active metallurgical agent essential for the TLPB process with a melting point (379–390 °C) significantly lower than the SSM 6063 substrate (616–654 °C) which make the Zamak 2 become a liquid phase at all process temperatures [6]. This liquid Zn-rich phase performs two critical functions:

1) Oxide Disruption: It facilitates the breakdown of the stable layer by penetrating micro-cracks and dissolving the Al substrate underneath it, causing the oxide to spall and be suspended in the molten Zn.
2) Isothermal Solidification: Al from the substrate dissolves into the liquid Zn, raising its liquidus temperature. This forces the liquid to solidify at the bonding temperature by precipitating Al-Zn intermetallic compounds (IMCs), such as $ZnAl_2$.

Jun-Xiang Wang et al. (2022) examined oxide evolution in solid-state welding and emphasized the need for advanced techniques to mitigate oxide-related bonding defects [7].

Di Zhao et al. (2023) demonstrated the effectiveness of ultrasonic-

* Corresponding author.
E-mail address: Chaiyoot.me@skru.ac.th (C. Meengam).

https://doi.org/10.1016/j.rineng.2025.108475
Received 23 May 2025; Received in revised form 10 November 2025; Accepted 27 November 2025
Available online 29 November 2025

assisted TLPB in disrupting oxide films and improving interfacial bonding strength [8]. Similarly, Zheyuan Huang et al. (2018) explored the application of Zn-Al interlayers in TLPB, highlighting the advantages of aluminum-zinc solubility in enhancing oxide dissolution [9]. In addition, a recent research by Meengam et al., (2023) on joint dissimilar diffusion bonding of SSM-ADC12 Al alloy to SSM 6063 Al alloy has further contributed to understanding the diffusion characteristics in aluminum alloy bonding, emphasizing the role of dissimilar materials in influencing oxide dissolution and bonding kinetics [10]. Despite these advancements, limited research has been conducted on the oxide behavior in TLPB of SSM 6063 aluminum alloy using Zamak 2 as a binder [11]. The lack of in-depth analysis of oxide dissolution kinetics and interfacial diffusion mechanisms presents a critical research gap that must be addressed.

This study aims to bridge this gap by systematically investigating the evolution and dissolution of oxide layers in the TLPB process for SSM 6063 aluminum alloy with Zamak 2 binder. Through comprehensive microstructural characterization and mechanical testing, this research will provide critical insights into the optimization of processing conditions for oxide-free, high-strength aluminum bonding. The findings are expected to advance the fundamental understanding of diffusion-driven oxide dissolution and contribute to the development of more efficient metallurgical bonding techniques for lightweight structural applications such as in automobile industry.

2. Related work & background

Recent research has provided valuable insights into oxide layer evolution and dissolution during TLPB, particularly in aluminum alloys. Canyu Liu et al. (2022) investigated ultrasonic-assisted TLPB of SiC ceramic and aluminum alloy, demonstrating how Zn interlayers improve bonding efficiency by disrupting oxide films, ultimately enhancing metallurgical bonding [12]. Similarly, Qiang Jia et al. (2020) explored Zn-Al interlayers in TLPB of 6061 Al alloy, showing their role in facilitating oxide breakdown and improving joint strength [13]. Zilong Guo et al. (2024) examined Cu/Al TLPB, emphasizing the importance of interlayer selection in controlling oxide dissolution kinetics [14]. Furthermore, Qiuyue Fang et al. (2023) highlighted the role of ultrasound-assisted TLPB in accelerating oxide disruption and metallurgical bonding in Al-Si alloys [15]. Beyond aluminum-based systems, William Reeks et al. (2020) analyzed nickel-based alloy TLPB, offering insights into oxidation resistance and interfacial reactions [16]. Finally, Ruaa Hatem Kadhim et al. (2024) introduced a two-step heating process to enhance oxide dissolution in aluminum alloy TLPB, highlighting its impact on interfacial diffusion [17]. These studies collectively reinforce the importance of optimized processing techniques to mitigate oxide-related defects and improve bonding performance in TLPB.

3. Methodology

3.1. Materials and specimen preparation

The SSM 6063 aluminum alloy was selected as the base material due to its excellent mechanical properties and corrosion resistance. The SSM 6063 aluminum alloy utilized in this experiment was specially manufactured with the Gas-Induced Semi-Solid (GISS) technique by J. Wannasin et al. (2010) [18]. On the other hand, the Zamak 2 (AC43A Zinc Alloy) was used as the binder material to facilitate metallurgical bonding and enhance oxide dissolution. The chemical compositions of SSM 6063 aluminum alloy and Zamak 2 are detailed in Table 1. The melting points of the materials in question are as follows: 616–654 °C (1140–1210 °F) from SSM 6063 aluminum alloy and 379–390 °C (714–734 °F) from Zamak 2 was exhibited. Both Specimens were machined to cylindrical shape. The dimensions of SSM 6063 aluminum alloy at Ø10×40 mm and Zamak 2 are at Ø10×0.5 mm respectively. The preparation of aluminum surfaces is a critical step in TLPB Bonding to ensure strong metallurgical bonding and minimize defects. The preparation of the bonding surfaces was a critical, multi-step process, performed as follows: specimen surfaces were first mechanically dried ground using P1200 grit SiC paper to remove the as-received oxide film and create a flat, uniform surface. Following this, the specimens were ultrasonically cleaned in pure acetone for 40 s to remove organic contaminants and polishing debris, then rinsed in deionized water for 60 s. To remove the native oxide layer, specimens were subsequently immersed in a 2 % HF solution for 60 s to remove pre-existing oxide layers to ensure complete surface purification. Immediately after etching, the specimens were submerged in a bath of deionized water for 3 min] to stop the etching reaction and remove residual acid. Finally, to minimize re-oxidation of the highly active aluminum surface, the prepared specimens were loaded into the argon-purged bonding chamber within 10 min of the final drying step.

3.2. Experimental setup

The prepared specimens are placed in an argon-purged chamber to prevent oxidation. In the horizontal diffusion bonding process, SSM 6063 aluminum alloy was positioned as the primary material. Simultaneously, Zamak 2 was centrally placed as the binder material. The experimental setup ensured that the materials were firmly pressed together under a bonding pressure of 4 MPa to promote diffusion bonding. To maintain a controlled atmosphere and prevent oxidation during TLPB process, argon gas was continuously introduced into the oven at a steady flow rate of 4 l per minute. This controlled environment facilitated effective bonding by minimizing contamination and ensuring uniform diffusion across the bonding interface. The temperature is gradually increased to 400–550 °C, exceeding the melting point of the interlayer but remaining below the solidus temperature of the base aluminum. The bonding time held at this temperature for 60 to 120 min, allowing the interlayer to diffuse into the base metal. Bonding times varied from 60 to 120 min to evaluate the effect of diffusion kinetics on oxide dissolution and protective argon atmosphere was employed to minimize re-oxidation during bonding. This thermal cycle diagram illustrates the temperature profile and bonding time for TLPB of aluminum alloys shown in Fig. 1.

The process consists of three main stages: heating, bonding, and cooling, with controlled parameters to optimize metallurgical bonding. The temperature gradually increases from room temperature (25 °C) to the bonding temperature, peaking at approximately 550 °C. This stage ensures the melting of the Zamak 2 interlayer, which facilitates the diffusion of zinc and aluminum atoms at the bond interface. During this stage, the molten interlayer gradually diffuses into the aluminum matrix, allowing for isothermal solidification and the formation of a strong metallurgical bond. Then, after the bonding process is complete, the temperature is gradually reduced back to room temperature. A controlled cooling rate is essential to minimize thermal stresses and prevent the formation of unwanted intermetallic compounds. The material solidifies, and the final microstructure of the bonded joint is determined. The step of the TLPB process is shown in Fig. 2.

Table 1
The chemical compositions of SSM 6063 aluminum alloy and Zamak 2 in the experiment (% by weight).

Element	Al	Mg	Si	Fe	Cu	Mn	Cr	Zn	Ti	Pb	Cd	Sn
SSM 6063 Al	Bal.	0.90	0.60	0.35	0.10	0.10	0.10	0.10	0.10	-	-	-
Zamak 2	3.7	0.06	-	0.05	3.30	-	-	Bal.	-	0.005	0.004	0.002

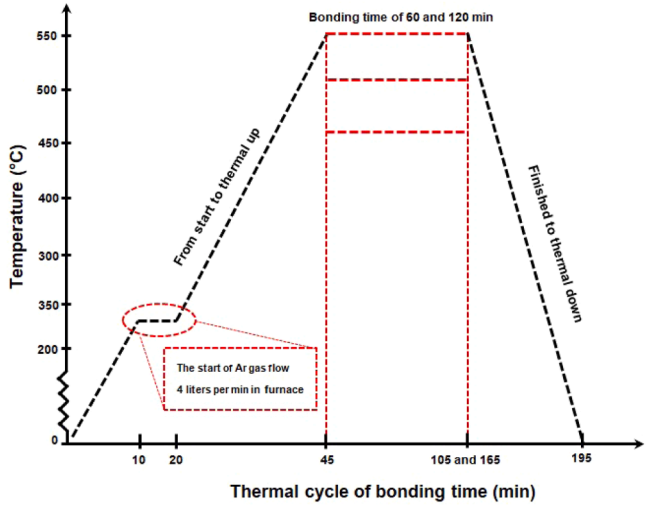

Fig. 1. The thermal cycle diagram of the TLPB process of SSM 6063 aluminum alloy with a Zamak 2 binder.

3.3. Microstructural elevation

After the TLPB process, the specimens were analyzed for residual oxide on the joint surface using the Energy Dispersive X-ray Spectroscopy (EDS) mode in a scanning electron microscope (SEM). The residual oxide test specimens were stored for a maximum of one week. Metallurgical analysis was conducted using an FEI-Quanta 400FEG SEM from Switzerland to examine elemental diffusion and distribution. Additionally, defects and grain transformation were observed using the Optika B-382PHi-ALC microscope from Italy. Prior to metallurgical analysis, the specimens' surfaces were prepared through sequential polishing with sandpaper of P320, P600, P800, P1000, and P1200 grit, followed by alumina powder polishing (3–5 μm), and finally etched using Keller's solution. Proper surface preparation is crucial for the TLPB welding process, particularly in removing contaminants from the joint surface and ensuring proper alignment of the bonding surfaces, as these factors significantly influence atomic diffusion during welding. The bonding strength and residual oxide content will be analyzed and reported. This study aims to evaluate the influence of residual oxide content on tensile strength variations and explore methods to minimize oxide formation during the welding process. Finally, Fractography analysis using SEM was performed to determine the fracture mechanisms and the influence of oxide remnants on bond failure.

3.4. Mechanical properties testing

The bonding strength specimens were prepared in accordance with the American Society for Testing and Materials (ASTM) E8 standard, which specifies the dimensions and geometry required for tensile testing of metallic materials. The tensile strength of the specimens was measured using a Testometric M500–25KN testing machine at room temperature, with a crosshead speed set to 1.67×10^2 mm per minute. According to ASTM-E8, the bonding strength of the specimens is shown in Fig. 3.

3.5. Validation and statistical

Based on the fundamental principles of transient liquid phase bonding, bonding temperature and bonding time are the two most critical processing parameters. These factors directly govern the diffusion kinetics, the rate of oxide dissolution, and the formation and growth of intermetallic compounds (IMCs), all of which determine the final joint integrity. Therefore, these two variables were selected as the main factors for this study.

This study investigates the TLPB of SSM 6063 aluminum alloy using AC43A Zinc Alloy (Zamak 2) as the binder. The experiment varies bonding temperature at 450, 500, and 550 °C and bonding time at 60 and 120 min while keeping bonding pressure at 4 MPa and argon gas flow rate at 4.8 L/min constant. A Full Factorial Design (3×2) with 3 replications (18 runs in total) was used. Minitab R17 was employed for DOE setup, randomization, and statistical analysis. The response variables (e.g., bonding strength, oxide thickness) were analyzed using ANOVA and interaction plots. The statistical significance of the factors and their interactions was evaluated using this ANOVA, with all tests conducted at a 95 % confidence level (alpha = 0.05). The goal is to determine the optimal bonding conditions for improved joint quality. The full factorial experiment with 3 replications (18 runs) and randomized run order of SSM 6063 aluminum alloy with Zamak 2 binder by TLPB process are detailed in Table 2.

4. Results and discussion

4.1. Characteristics of TLPB specimens

The characteristics of specimens from the bonding time of 120 min and bonding temperature 450, 500, and 550 °C are shown in Fig. 4. The

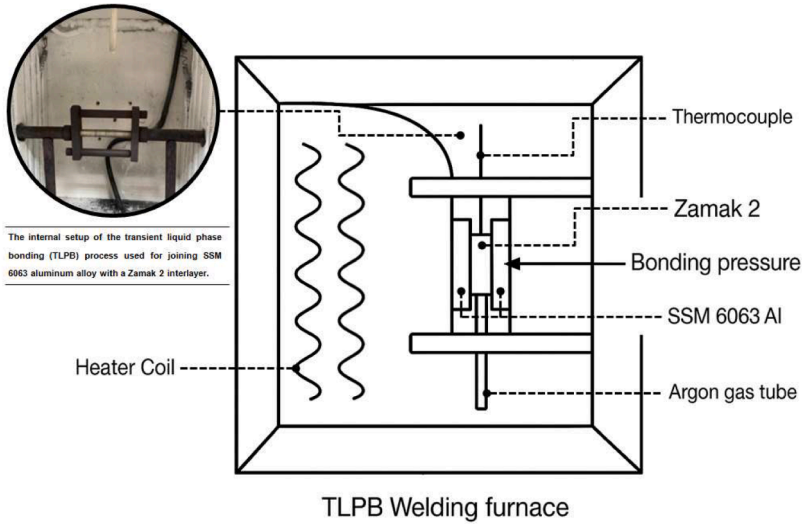

Fig. 2. The inside of the TLPB process furnace.

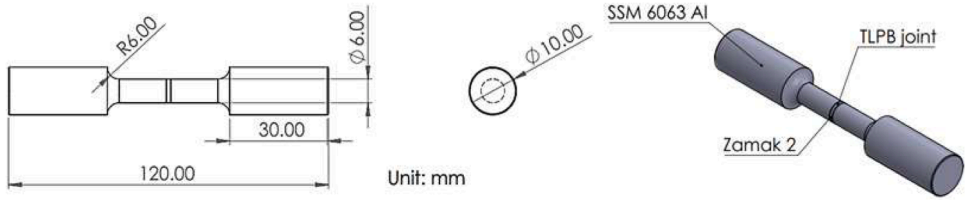

Fig. 3. The bonding strength specimens of ASTM-E8 standard.

Table 2
The full factorial design in the experiment of TLPB process of SSM 6063 aluminum alloy with Zamak 2 binder.

Run Order	Bonding Temperature (°C)	Bonding Time (min)	Replication
4	450	120	2
13	550	60	2
15	550	120	1
16	550	120	2
2	450	60	3
8	500	60	3
9	500	120	1
11	500	120	3
6	500	60	1
12	550	60	1
1	450	60	2
17	550	120	3
5	450	120	3
3	450	120	1
7	500	60	2
14	550	60	3
10	500	120	2
18	450	60	1

specimens represent different bonding temperature conditions while maintaining a constant bonding time of 120 min, affecting bond quality, intermetallic formation, and diffusion mechanisms. The specimen from 450 °C and 120 min exhibits the strongest bonding quality. Also, it can be noticed that the higher amount of flash material came out and assume that the liquidity of material has been mixed. This helps in oxide layer disruption and proper intermetallic compound (IMC) formation shown in Fig. 4(a). However, excessive heating may lead to thicker IMCs, affecting ductility. Han Jiang et al. (2022) and Yinghao Li et al. (2024) found that temperatures above 500 °C improve diffusion bonds while requiring control to prevent excessive IMC growth [19,1]. The specimen at 500 °C and 120 min has moderate bond strength, but partial oxidation and uneven IMC formation can introduce diffusion barriers, reducing joint uniformity shown in Fig. 4(b). Pu Zhao et al. (2023) emphasized the importance of oxide removal, as oxidation at intermediate temperatures hinders diffusion and leads to partial IMC formation, which may still contain inconsistencies [20]. The specimen at 550 °C and 120 min has the weakest bond quality. At this high temperature, **excessive oxidation and the rapid, uncontrolled growth of brittle IMCs** create a flawed joint, which hinders the formation of a sound metallurgical bond and residual oxides acting as diffusion barriers shown in Fig. 4(c). Zhongman Cai et al. (2025) indicated that lower temperatures often lead to weak bonding [21], and Chaiyoot Meengam et al. (2018) reported that bonding at 450 °C results in persistent oxide layers, reducing strength. Overall, 450 °C provides the strongest and most uniform bonding, 500 °C may require oxide removal treatments, and 550 °C should be avoided unless longer bonding times or diffusion enhancement methods are applied [22].

The characteristics of specimens from the bonding time of 60 min and bonding temperature 450, 500 and 550 °C are shown in Fig. 5. The specimen from 450 °C and 60 min shows the strongest bond with enhanced diffusion, minimal oxidation, and a well-defined interface, although shorter bonding time may result in thinner intermetallic layers shown in Fig. 5(a). The specimen at 500 °C and 60 min exhibits moderate bonding quality, with some oxidation and partial intermetallic formation, leading to potential diffusion barriers shown in Fig. 5(b). The specimen at 550 °C and 60 min has the weakest bond, with limited diffusion and residual oxides, resulting in poor mechanical integrity shown in Fig. 5(c).

4.2. Oxide dissolution evolution

The SEM-EDX analysis presents Energy-dispersive X-ray (EDX) analysis which was employed to characterize the microstructure and determine the damage mechanisms as comprehensive investigation into the microstructural characteristics of a bonded aluminum alloy joint [23]., likely processed via TLPB using Zn as an interlayer of the sample from 450 °C for 120 min as shown in Fig. 6. Fig. 6(a), a grayscale SEM micrograph, reveals a fractured or delaminated joint interface, suggesting the presence of either brittle intermetallic compounds (IMCs), residual oxides, or insufficient diffusion during bonding, which is consistent with previous findings on oxide-related bonding failures [24]. The EDS layered mapping in Fig. 6(b) illustrates a heterogeneous elemental distribution, with Zn, Al, O, and C unevenly dispersed, indicating incomplete diffusion or phase separation. The EDS spectrum in Fig. 6(c) identifies dominant Al and Zn peaks, confirming the presence of the Zn-based filler metal, while significant O and C peaks suggest oxidation and potential contamination, aligning with studies that report oxide-induced diffusion barriers in aluminum bonding [25]. The elemental mapping shown in Fig. 6(d)–(g) provides spatial distribution insights: (d) highlights carbon accumulation at the interface, which may

Fig. 4. The images welded cylindrical specimens which are likely bonded using TLPB of SSM 6063 aluminum alloy with Zamak 2 binder from the bonding time of 120 min as: (a) 450,
(b) 500 and (c) 550 °C.

Fig. 5. The images of welded cylindrical specimens which are likely bonded using TLPB of SSM 6063 aluminum alloy with Zamak 2 binder from the bonding time of 60 min as: (a) 450,
(b) 500 and (c) 550 °C.

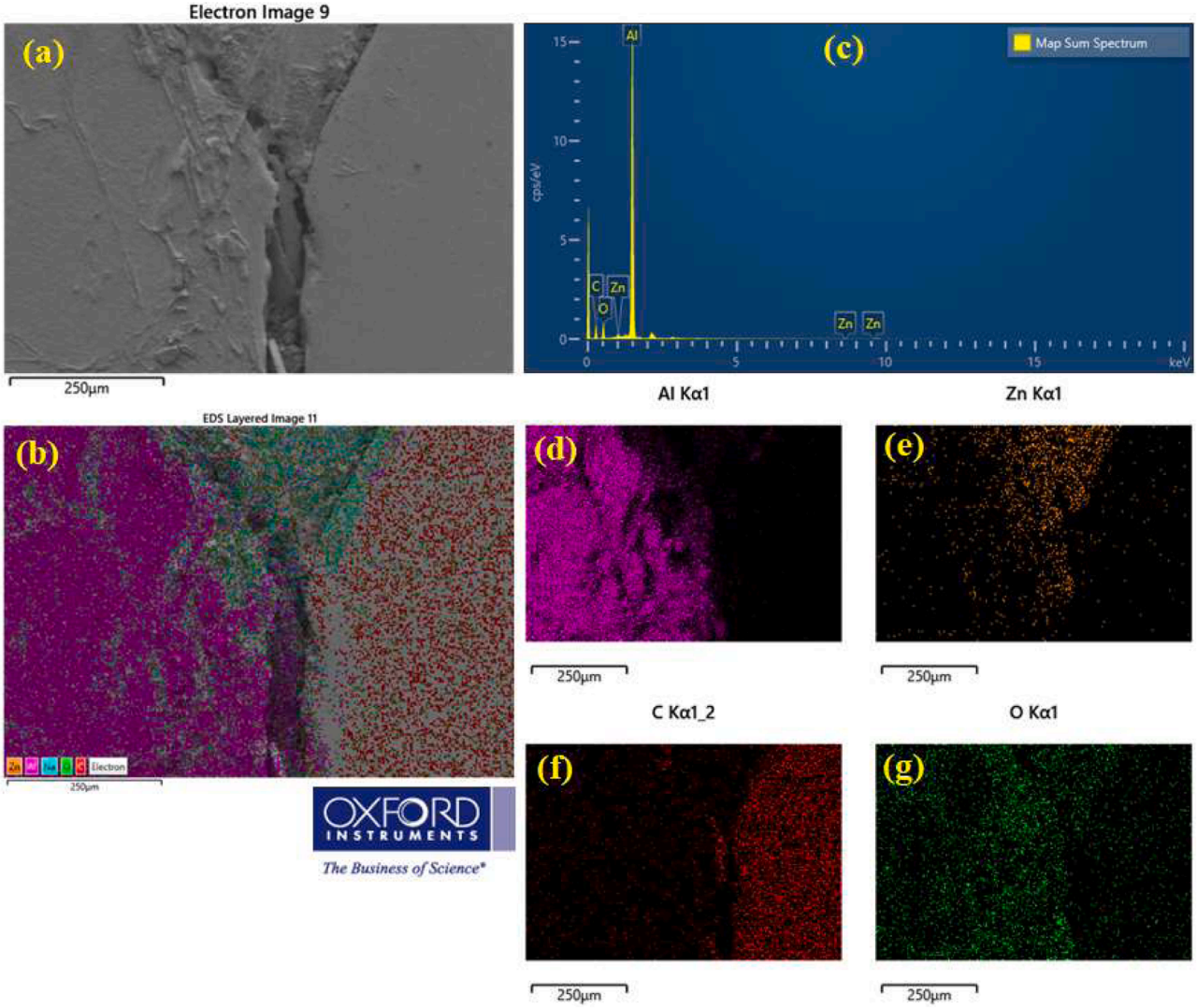

Fig. 6. The SEM micrograph and EDS analysis of Zn-assisted TLPB in an aluminum alloy from the sample of 450 °C for 120 min. (a) SEM image shows a void at the bonding interface, (b) EDS mapping illustrates elemental distribution, (c) EDS spectrum confirms Al and Zn as major elements, with C and O peaks suggesting contamination or oxidation, (d) Al concentration at the interface, (e) Non-uniform Zn distribution, (f) Elemental maps show carbon accumulation, and (g) oxide-rich regions, and increase O elements at the interface, indicating diffusion barriers and IMC formation. All of the above figures are from running order # 4.

be attributed to organic contaminants or decomposition of binder residues, hindering atomic diffusion. Fig. 6(e) exhibits oxygen-rich regions, indicative of oxide formation (likely Al_2O_3 or ZnO), which can significantly weaken joint integrity [26]. Fig. 6(f) shows Zn concentration at the bonding interface, which, suggests segregation or non-uniform isothermal solidification. As explained by the TLPB mechanism, this solidification proceeds via the formation of *Al-Zn* intermetallic. In this case, the brittle $ZnAl_2$ phase is formed. This observation is critical, as it supports our hypothesis. And, Fig. 6(g) illustrates the aluminum matrix, with a reduced concentration near the interface, possibly due to diffusion into the Zn phase or reaction with oxides [27]. The presence of fractures in Fig. 6(a) corroborates the hypothesis of brittle IMC formation, commonly observed in Zn-assisted TLPB processes. These findings emphasize the critical role of oxide management, optimized bonding parameters, and controlled Zn diffusion to enhance joint strength and structural integrity, which is supported by prior research on Al-Zn diffusion bonding mechanisms [28].

Table 3 shows the elemental composition analysis from EDS data revealing significant variations in carbon (C), oxygen (O), aluminum (Al), and zinc (Zn) concentrations across different bonding temperatures (450, 500, and 550 °C), influencing joint integrity. At bonding temperatures of 450 °C, carbon is the highest (57.03 Wt %), indicating surface contamination, while aluminum remains low (24.09 Wt %). Oxygen content (16.40 Wt %) is moderate, while zinc is minimal (0.43 Wt %), due to the temperature is hot enough to disrupt the oxide and complete the TLPB diffusion (consuming the liquid Zn). At 500 °C, aluminum reaches its peak (42.37 Wt %), with a reduction in carbon (40.69 Wt %) and oxygen (18.48 Wt %), indicating improved bonding conditions (Meengam et al., 2024). However, at 550 °C, oxygen increases sharply (28.90 Wt %), forming thicker oxide layers that hinder diffusion, while Zn accumulation (16.35 Wt %) suggests brittle intermetallic phase formation [29]. The significant Al reduction (17.26 Wt %) at 550 °C implies the reaction with Zn and O, leading to $ZnAl_2$ intermetallics, which can compromise joint strength [30]. Therefore, these findings from the EDS trends, when interpreted correctly, confirm that 450 °C is the optimal temperature. It provides the ideal kinetic balance: it is hot enough to disrupt the oxide and complete the TLPB diffusion (consuming the liquid Zn), but cool enough to prevent both excessive oxidation and the growth of thick, brittle $ZnAl_2$ IMCs. The high carbon at 450 °C is attributed to surface contamination during the post-fracture analysis and is not considered representative of the bulk joint mechanism. In short, this data must be interpreted not in terms of total

Table 3
The concentration of elements from the bonding time at 120 min by EDS technique from SEM were measured.

TLPB parameter	Element	Line Type	Apparent Concentration	k Ratio	Wt %	Wt % Sigma	Atomic %	Standard Label
450 °C	C	K series	0.28	0.02078	57.03	0.47	69.81	C Vit
	O	K series	1.65	0.00551	16.40	0.38	16.96	SiO_2
	Al	K series	6.53	0.04693	24.09	0.26	13.13	Al_2O_3
	Zn	K series	0.09	0.00095	0.43	0.09	0.10	Zn
	Total:				100		100	
500°C	C	K series	0.48	0.00481	40.69	0.73	56.54	C Vit
	O	K series	0.87	0.00292	18.48	0.41	17.11	SiO_2
	Al	K series	6.33	0.04543	42.37	0.54	26.21	Al_2O_3
	Zn	K series	0.06	0.00064	0.55	0.11	0.14	Zn
	Total:				100		100	
550 °C	C	K series	0.71	0.00713	37.47	1.02	53.66	C Vit
	O	K series	2.11	0.00710	28.90	0.85	31.05	SiO_2
	Al	K series	0.88	0.00635	17.26	0.75	10.99	Al_2O_3
	Zn	K series	4.05	0.00446	16.35	0.90	4.30	Zn
	Total:				100		100	

diffusion, but in how the process parameters achieved the TLPB goals: oxide disruption and successful isothermal solidification.

This Scanning Electron Microscope (SEM) image captures a TLPB joint between SSM 6063 aluminum alloy and Zamak 2 (AC43A zinc alloy) as shown in Fig. 7, taken at 1,000X magnification and 5.00 kV with an ETD detector, showing critical microstructural features such as oxide layers and cracks at the bonding interface. A significant crack along the bonding edge suggests weak adhesion and fracture propagation, likely caused by residual oxides, thermal stress, and brittle intermetallic compounds (IMCs). The expansion of aluminum oxide (Al_2O_3) has contributed to localized tensile stress, leading to the formation of interfacial cracks, poor diffusion, and weak joint integrity. Fragmented structures near the crack edge indicate intermetallic phase formation, likely Al-Zn or Al-Zn-Cu IMCs, which are brittle and promote stress concentration, accelerating failure. Chidinma Imediegwu et al. (2022) found that the higher bonding temperatures (above 500 °C) can improve diffusion but must be controlled to prevent excessive IMC growth [31]. G.O. Cook et al. (2011) emphasized the need for oxide removal to prevent crack formation is recommended pre-bonding surface treatments like mechanical polishing or plasma cleaning [32]. M.K. Pal et al. (2023) highlighted that higher bonding pressures (4–6 MPa) reduce voids and cracks, improving overall joint integrity [33]. Final recommendations include oxide removal treatments, increased bonding pressure (4–6 MPa), and optimized bonding temperatures above 500 °C to minimize cracking and enhance the mechanical performance of the joint are shown in Fig. 7.

It is important to place these oxide-related findings within the broader context of aluminum joining. The process used in this study—a chemical pre-clean followed by bonding in an argon atmosphere —is a common industrial approach that aims to *minimize* re-oxidation in a cost-effective manner.

This contrasts with flux-assisted methods, which use chemically aggressive fluxes to actively dissolve the aluminium oxide layer. While highly effective, flux-assisted bonding introduces significant challenges, as the corrosive residues require a difficult and critical post-bond cleaning step to prevent long-term joint degradation.

Alternatively, high-vacuum bonding, often combined with *in-situ* sputter-cleaning, can eliminate oxide barriers by preventing their re-formation entirely. However, the high capital cost and batch-processing nature of vacuum furnaces often make this approach less suitable for the high-volume, low-cost demands of the automotive industry.

Therefore, the process in our study represents an industrial compromise. It relies heavily on the *in-situ* metallurgical action of the liquid Zamak 2 to disrupt and disperse the residual oxide, which our results show is a key mechanism that must be precisely controlled to achieve a reliable joint.

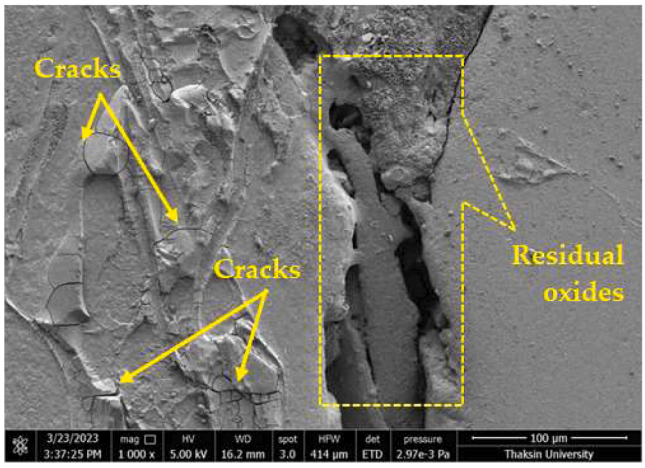

Fig. 7. The SEM image at the edges of the joint using TLPB of SSM 6063 aluminum alloy with Zamak 2 binder from the sample of 450 °C for 120 min. The above figures are from running order # 4.

4.3. Microstructural analysis

The SEM micrographs shown in Fig. 8(a)–(f) reveal distinct microstructural characteristics and bonding defects in Zn-assisted TLPB of aluminum alloys, highlighting issues related to diffusion, oxidation, and intermetallic compound (IMC) formation. Fig. 8(a) shows interfacial separation, suggesting brittle failure due to residual oxides and insufficient Zn-Al diffusion, which aligns with findings by H. Jiang et al. (2011) on oxide-induced weak joints [34]. Fig. 8(b) presents porosity and voids, likely caused by incomplete diffusion, entrapped gases, or shrinkage effects, consistent with Zhenqian Lang et al. (2024), who identified microporosity in Al-Zn bonding [35]. Fig. 8(c) shows interfacial separation, indicating weak metallurgical bonding due to low bonding pressure and diffusion barriers [36]. Fig. 8(d) depicts needle-like Zn-rich IMCs ($ZnAl_2$), which form at high temperatures, increasing hardness but reducing ductility [37]. Fig. 8(e) displays a smooth, defect-free bond interface, suggesting optimized bonding at 450 °C, where oxide disruption allows effective diffusion. Lastly, Fig. 8(f) shows surface contamination and oxidation, likely due to inadequate surface preparation and environmental exposure, reinforcing findings on oxide impact in Al bonding [38].

4.4. Mechanical properties

The presented graph illustrates the influence of bonding temperature and bonding time on the bonding strength of TLPB shown in Fig. 9(a). The bonding strength exhibits a decreasing trend with an increase in

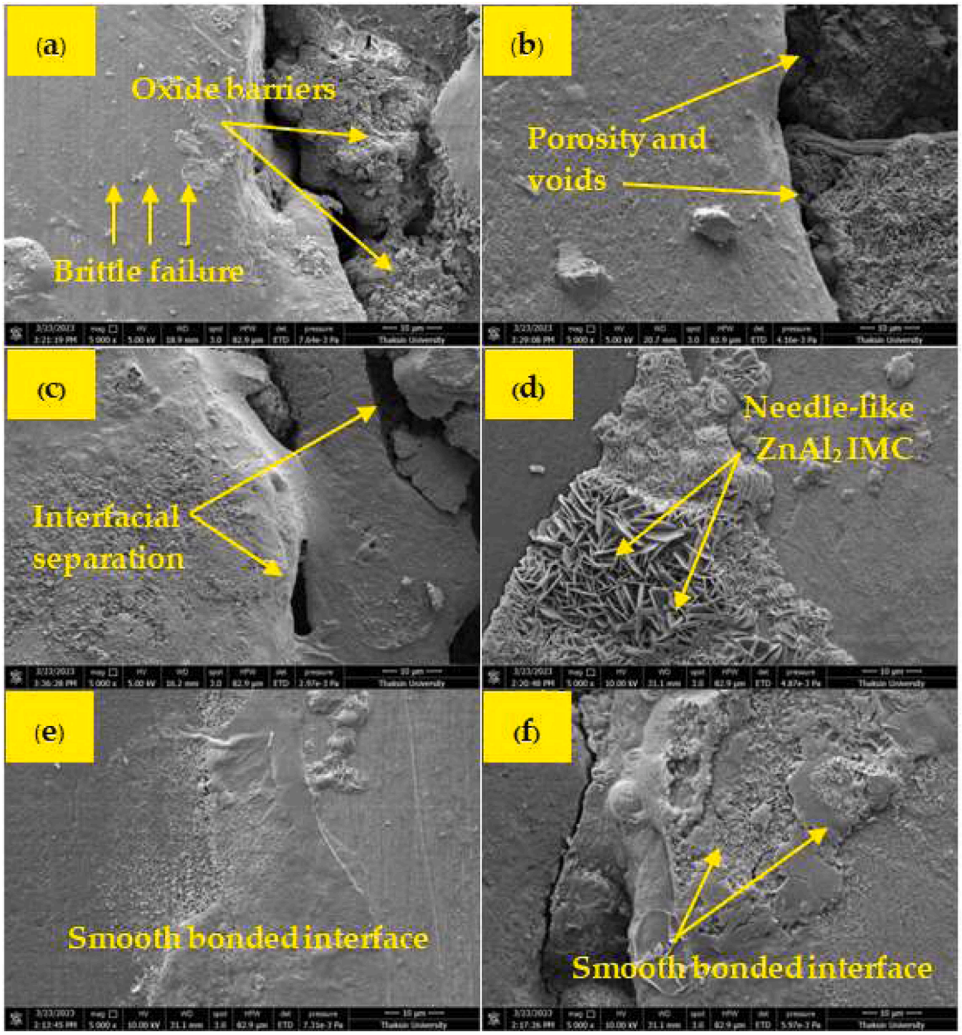

Fig. 8. SEM Micrographs of bonded aluminum alloy joints in zn-assisted TLPB; (a) Cracked bond interface, indicating brittle failure and oxide barriers. (b) Porosity and voids, (c) Interfacial separation, (d) Needle-like $ZnAl_2$ intermetallic compounds. (e) Smooth, well-bonded interface and (f) Surface oxidation and contamination. All of the above figures are from running order # 4 from the condition of 450 °C at 120 min.

temperature, which is more pronounced at a prolonged bonding time of 120 min compared to 60 min. At a bonding temperature of 450 °C, the bonding strength is at its peak for both bonding times, with 120 min yielding a higher initial strength than 60 min having a bonding strength of 23.56 ± 3.4 MPa, but at 60 min has a bonding strength of 19.99 ± 3.2 MPa. However, when the temperature rises beyond 450 °C, a substantial drop in bonding strength was observed, particularly for the 120 min bonding time leading to having bonding strength of 10.11 ± 4.9 MPa was the minimum for all conditions. This decline is a direct consequence of the TLPB mechanism kinetics. While the process relies on the formation of *Al-Zn* intermetallic, excessive thermal energy accelerates this pathway detrimentally. At 450 °C, the kinetics are slow enough to allow for oxide disruption while growing only a thin, controlled $ZnAl_2$ IMC layer, resulting in the optimal joint strength. Conversely, at 550 °C, the kinetics are too rapid. This leads to the excessive growth of a thick, brittle $ZnAl_2$ layer, as suggested by the high Zn concentration and the needle-like IMCs observed. This, combined with the severe oxidation that forms a continuous barrier, explains the catastrophic drop in mechanical strength. This decline suggests that excessive thermal exposure may exacerbate grain coarsening, interfacial void formation, or oxide layer accumulation, leading to deterioration in mechanical properties by Xin Zhang et al. (2025) [39]. The result indicates the oxide volume in experimental measurements, found that the bonding time and bonding temperature lower resulting in less oxide content, but relatively maintains bonding strength. This suggests that prolonged thermal exposure may facilitate detrimental diffusion processes, weakening the joint integrity. The results align with existing literature, where the interplay between temperature and bonding time significantly affects joint microstructure [40]., diffusion kinetics and resultant mechanical performance [41]. Existing previous studies in the domain of TLPB have highlighted the importance of optimizing bonding parameters to achieve superior mechanical properties. For instance, diffusion-driven bonding kinetics have been extensively analyzed in studies exploring Al-based alloys, where the oxide layer evolution and intermetallic formation play a crucial role in joint strength. Other works have emphasized the role of alloying elements in mitigating brittle phase formation, leading to enhanced ductility. Additionally, the dissolution and re-precipitation mechanisms of intermetallic compounds under varying bonding conditions have been a focal point in recent research. Comparative assessments of solid-state diffusion and liquid-assisted diffusion mechanisms indicate that optimized temperature-time combinations can significantly improve joint uniformity [42]. Finally, several investigations into process modeling have provided insights into the prediction of interfacial evolution and long-term reliability of TLPB joints, reinforcing the importance of parameter optimization for industrial applications. The study examines how bonding temperature and time influence oxide volume in TLPB [43]. The results show that oxide volume increases with temperature, with a more significant rise

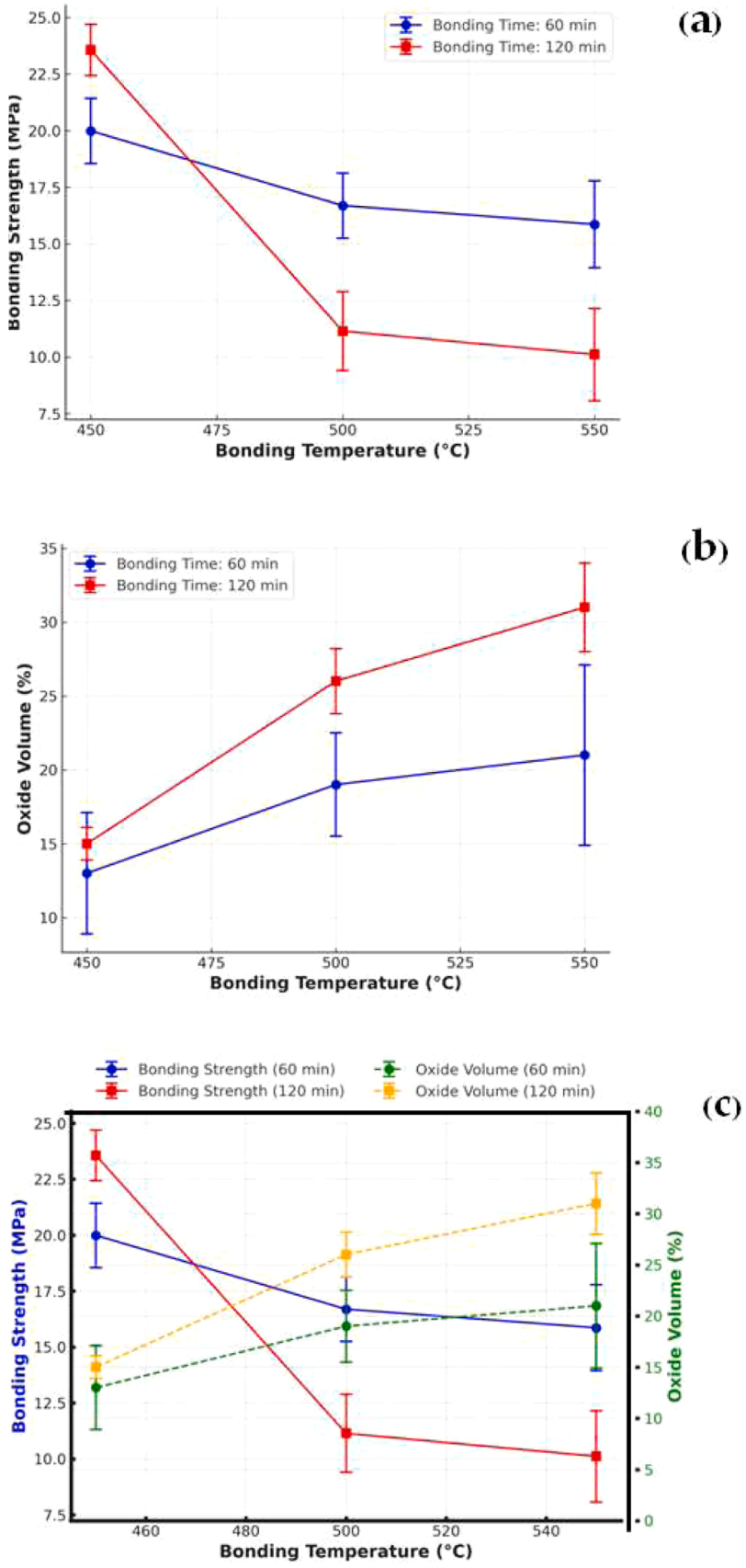

Fig. 9. The results of bonded strength and Oxide volume with standard deviation bars from bonding temperature and bonding time of TLPB of SSM 6063 aluminum alloy with Zamak 2 binder.

observed at a prolonged bonding time of 120 min compared to 60 min. At 450 °C, oxide formation is minimal (12–15 %), but as the temperature increases, oxidation intensifies, peaking at 550 °C. The 120 min bonding time consistently produces more oxide than the 60 min bonding time, indicating prolonged thermal exposure accelerates oxidation. The increase in oxide volume was attributed to enhanced diffusion and reaction kinetics, facilitating oxygen penetration at elevated temperatures [44]. Prolonged bonding times further promote oxidation, leading to excessive oxide accumulation that can weaken joint integrity. These findings align with established diffusion bonding studies, confirming the correlation between bonding temperature, time, and oxidation-related degradation. Comparative studies highlight similar trends in oxide formation in aluminum alloys and diffusion bonding. This research shows that prolonged exposure fosters continuous oxide layer growth, which impedes atomic bonding and reduces mechanical performance. Strategies such as flux-assisted bonding and surface pre-treatment have been explored to mitigate oxidation. Numerical models predict oxidation kinetics, correlating process conditions with oxide accumulation and joint properties. Advanced characterization techniques, like in-situ synchrotron analysis, validate these trends, emphasizing the need to control bonding conditions to minimize oxidation and enhance joint reliability shown in Fig. 9(b). The study investigates the effects of bonding temperature and time on bonding strength and oxide volume in TLPB. Results reveal an inverse relationship: bonding strength decreases as oxide volume increases, particularly at 120 min bonding times. At 450 °C, bonding strength is the highest, but it declines significantly at 550 °C, with oxide volume exceeds 30 %. The 60 min bonding time exhibits a more gradual strength reduction and lower oxidation. Excessive oxidation at high temperatures impairs atomic diffusion and weakens joint integrity [45]. Variations in oxide formation and strength indicate microstructural inconsistencies. Comparative studies confirm that prolonged exposure promotes oxidation, reducing mechanical performance. Mitigation techniques like flux-assisted bonding and optimized atmospheres help control oxide growth. Computational models and in-situ analysis further validate oxidation kinetics and bonding behavior, emphasizing the need for precise parameter control shown in Fig. 9(c).

4.5. Statistical analysis

The ANOVA results indicate that bonding temperature is the most influential factor ($p = 0.00001$, $F = 35.31$) in determining the response, followed by bonding time ($p = 0.01729$, $F = 7.62$), though its effect is smaller. However, the interaction between bonding temperature and bonding time is statistically significant ($p = 0.00215$, $F = 10.70$), meaning these factors influence each other rather than acting independently. The model explains 89.26 % of the total variation (R-Sq), with an adjusted R-Sq of 86.15 % and a predicted R-Sq of 80.42 %, confirming its reliability for prediction (Alpha value at 0.05 with confident level 95 %). The low residual error (MS = 3.95) and standard deviation ($S = 1.98$) suggest a well-fitting model. These results emphasize that optimizing bonding temperature is the primary priority, but bonding time should also be adjusted in combination to achieve the best results. The interaction effect highlights the need to consider both factors together rather than separately when optimizing process conditions. In this experiment, bonding temperature and bonding time are controllable variables since they can be directly adjusted during the process to optimize the outcome. Controllable variables can regulate to achieve the desired results, such as heating rate, pressure, and holding time in diffusion bonding. However, uncontrollable variables are factors that cannot be easily adjusted or eliminated but still influence the results. These may include oxide layer thickness on the aluminum surface, microstructural variations in the material, and atmospheric conditions [46]. Understanding these uncontrollable variables is crucial because they introduce variability into the process and can impact bonding strength, defect formation, and overall joint quality as detailed in Table 4.

The 3D response surface plot shows that bonding temperature and bonding time significantly influence bonding strength in diffusion bonding. Bonding strength increases with temperature down to about 450 °C due to enhanced atomic diffusion, which disrupts oxide layers and improves metallurgical bonding. However, beyond 525 °C, bonding strength decreases due to overheating, which causes grain coarsening, oxidation, or even localized melting, leading to weaker joints [47]. Bonding time also plays a crucial role, with shorter times (~60 min) at moderate temperatures resulting in higher bonding strength [48]. This is because adequate diffusion occurs without excessive grain growth or intermetallic formation. In contrast, prolonged times (>100 min) reduce bonding strength due to excessive grain coarsening or brittle intermetallic compounds. The plot shows a significant interaction effect between bonding temperature and time, revealing that the impact of bonding time depends on the temperature level. Optimal bonding strength (~25 MPa) was achieved at 450 °C and 120 min, balancing enhanced diffusion with minimal adverse effects. The interaction effect suggests a synergistic relationship, requiring temperature and time to be optimized together. Bonding temperature is the most influential factor, but its impact is strongly linked to bonding time. Therefore, excessive times at high temperatures should be avoided to prevent grain coarsening and oxidation [49]. The findings emphasize that a balanced optimization approach considering both main effects and interactions is necessary for maximizing bonding strength. These results align with the diffusion bonding mechanism, where atomic mobility depends on temperature, and bonding time influences diffusion extent and microstructure evolution. The analysis highlights the need for precision control of bonding parameters to enhance joint strength and material performance in diffusion bonding applications as shown in Fig. 10.

The contour plot shows that bonding temperature and bonding time significantly affect bonding strength in diffusion bonding. Bonding strength increases with temperature up to about 450 °C, which disrupts oxide layers and improves metallurgical bonding. However, beyond 525 °C, bonding strength decreases because of overheating, leading to grain coarsening, oxidation, cracking, or partial melting that weakens the joint [50]. Shorter bonding times (60–80 min) at moderate temperatures yield higher bonding strength as they provide sufficient diffusion time without excessive grain growth or intermetallic formation. Conversely, longer bonding times (>100 min) can decrease strength due to excessive grain growth or brittle intermetallic compounds. The contour lines' nonlinear pattern indicates a significant interaction between bonding temperature and bonding time, showing that the bonding time's effect depends on the temperature level. Optimal bonding strength (~23.2 MPa) was achieved at 450 °C and 100–120 min, balancing diffusion with minimal adverse effects. At higher temperatures (~525–550 °C), bonding strength remains low regardless of time due to high thermal energy for overheating, leading to grain coarsening, oxidation, cracking, or partial melting. The interaction effect suggests a synergistic relationship requiring the joint optimization of temperature and time. Temperature is the most influential factor, but its effect is highly interactive with bonding time, emphasizing the need for a balanced

Table 4
The analysis of variance (ANOVA) of SSM 6063 aluminum alloy with Zamak 2 binder with TLPB process.

Source	Sum of Squares (SS)	df	Adj SS	Adj MS	F-value	P-value
Bonding temperature	278.93	2	278.93	139.47	35.31	0.00001
Bonding time	30.08	1	30.08	30.08	7.62	0.01729
Bonding temperature × Bonding time	84.55	2	84.55	42.27	10.70	0.00215
Error	47.40	12	47.40	3.95		
Total	441.00	17				

$S = 1.98$, R-Sq = 89.26 %, R-Sq(adj) = 86.15 %, R-Sq(pred) = 80.42 %ky.

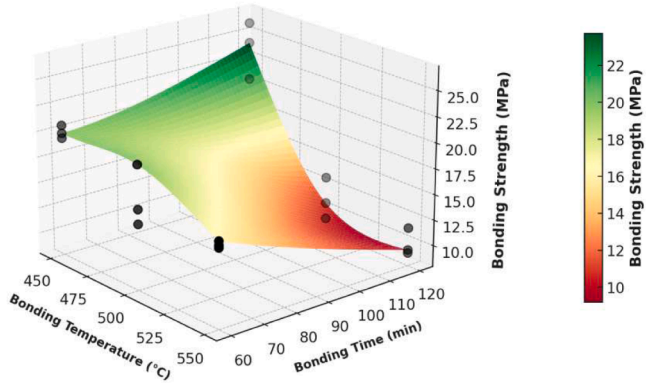

Fig. 10. The 3D response surface plot illustrates the relationship between Bonding Temperature (°C), Bonding Time (min), and Bonding Strength (MPa) of TLPB of SSM 6063 aluminum alloy with Zamak 2 binder.

optimization approach. The steep contour gradient near 525 °C indicates that bonding strength is extremely sensitive to temperature changes, requiring precise temperature control. The results align with the diffusion bonding mechanism, where temperature drives atomic diffusion while time controls the extent of diffusion and microstructure evolution [51]. Excessive times at high temperatures should be avoided to prevent grain coarsening and oxidation. These findings emphasize the importance of optimizing both parameters together for maximum bonding strength as shown in Fig. 11.

This equation is a second-order polynomial regression model, commonly used in Response Surface Methodology (RSM) for multi-response optimization. It predicts the response variable(s) (e.g., bonding strength, hardness) under different combinations of bonding temperature (T) and bonding time (t). The goal is to find the optimal process parameters that maximize or minimize the response(s). Multi-response optimization is crucial in industrial processes like diffusion bonding, where multiple output characteristics (e.g., bonding strength, joint integrity, and ductility) must be optimized simultaneously. This model is particularly useful because it accounts for non-linear effects and interactions, providing a more accurate representation of the system's behavior. The mathematical formulation for multi-response optimization is expressed as:

$$Y = f(T, t) = A0 + A1\,T + A2\,t + A3\,T^2 + A4(T \times t) + A5\,t^2 \quad (1)$$

When

Y = Response variable (e.g., bonding strength)

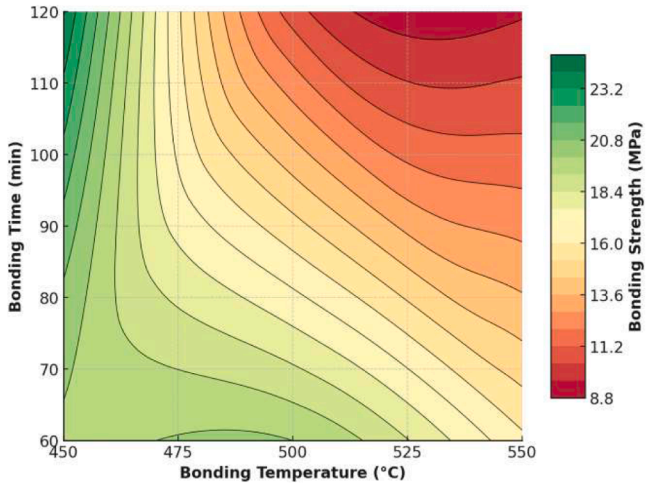

Fig. 11. The contour plot from TLPB parameters of SSM 6063 aluminum alloy with Zamak 2 binder.

T = Bonding temperature (°C)

t = Bonding time (min)

This polynomial regression model provides an advanced analytical tool for predicting both bonding strength and oxide volume with high precision. This model enables multi-objective optimization, balancing high bonding strength and low oxide volume, which is crucial in diffusion bonding and transient liquid phase bonding. The bonding strength mathematical formulation for multi-response optimization is expressed as:

$$\begin{aligned}\text{Bonding Strength} = {} & 367.0632 + (-1.3317 \times T) + (0.0000 \times t) \\ & + (0.0014 \times T^2) + (-0.0015 \times T \times t) \\ & + (0.0041 \times t^2)\end{aligned} \quad (2)$$

The bonding strength equation models the relationship between bonding temperature (T) and bonding time (t) using a second-order polynomial regression, capturing linear, quadratic, and interaction effects. The negative linear coefficient for temperature (−1.3317) indicates that increasing temperature linearly decreases bonding strength, likely due to overheating effects like grain coarsening or oxidation. The zero linear coefficient for bonding time suggests that time alone does not significantly impact bonding strength but affects it through non-linear and interaction effects. The positive quadratic terms for both temperature and time show U-shaped relationships, indicating that bonding strength initially decreases but then levels off or increases at extreme values. This reflects complex thermal and diffusion mechanisms where optimal bonding occurs within a specific range, and excessive values lead to adverse microstructural changes. The negative interaction term (−0.0015) indicates an antagonistic relationship, meaning that high temperatures combined with long bonding times reduce bonding strength, likely due to over-diffusion or brittle intermetallic compounds. The model highlights the need for joint optimization of temperature and time [52], as their effects are not independent. This equation is valuable for predicting bonding strength and optimizing diffusion bonding processes by identifying the optimal balance of temperature and time [53].

While, the oxide volume equation models the relationship between bonding temperature (T) and bonding time (t) using a second-order polynomial regression, capturing linear, quadratic, and interaction effects. The positive linear coefficient for temperature (0.9700) shows that increasing temperature directly increases oxide volume due to enhanced oxidation rates at higher temperatures. The zero linear coefficient for bonding time indicates that time alone does not significantly affect oxide volume but influences it through non-linear and interaction effects. The negative quadratic term for temperature (−0.0010) suggests a parabolic relationship, where oxide volume initially increases but decreases at extremely high temperatures due to oxide instability or evaporation. The negative quadratic term for bonding time (−0.0030) indicates that oxide volume initially increases and then stabilizes or decreases as the oxide layer thickens and diffusion slows down. The positive interaction term (0.0013) shows a synergistic effect, where the elevated temperatures combined with long time maximize oxide volume, reflecting temperature-dependent diffusion mechanisms [54]. The model emphasizes that temperature and time are not independent and must be optimized together to control oxide formation effectively. It enables prediction, optimization, and sensitivity analysis for oxide volume in diffusion bonding, supporting process control and improved joint quality. The oxide volume mathematical formulation for multi-response optimization is expressed as:

$$\begin{aligned}\text{Oxide Volume } (\%) = {} & -251.7586 + (0.9700 \times T) + (-0.0000 \times t) \\ & + (-0.0010 \times T^2) + (0.0013 \times T \times t) \\ & + (-0.0030 \times t^2)\end{aligned} \quad (3)$$

To develop an optimal predictive model that simultaneously estimates bonding strength (MPa) and oxide volume (%), this approach provides a comprehensive understanding of how bonding parameters

influence both responses. A single mathematical model incorporating both bonding strength (BS) and oxide volume (OV) as functions of Bonding Temperature (T) and Bonding Time (t) is formulated as:

$$\begin{aligned}[BS+OV] = w1\big[& \\ & -\left(367.0632-1.3317T+0.0014T^2-0.0015Tt+0.0041t^2\right)\big] \\ & +w2\big[\\ & -251.7586+0.9700T-0.0010T^2+0.0013Tt-0.0030t^2\big]\end{aligned} \tag{4}$$

In this study, w1 represents the weight assigned to maximizing bonding strength, while w2 corresponds to minimizing oxide volume. Both weights are positive real numbers and are constrained to sum to unity (i.e., w1+w2 = 1). In this multi-response model, the weights w1 and w2 represent the industrial priority assigned to each objective. The selection of these weights is a critical engineering decision:

- Assigning a higher weight to w1 (e.g., w1= 0.7, w2= 0.3) prioritizes maximum initial bonding strength, which may be suitable for static, non-critical components.
- Assigning a higher weight to w2 (e.g., w1= 0.3, w2= 0.7) prioritizes minimum oxide volume. This is the more likely scenario for automotive applications, as residual oxides act as initiation sites for fatigue, cracking, and corrosion, making their minimization essential for long-term reliability.

A sensitivity analysis was conducted to evaluate how the choice of these weights affects the optimal process parameters. This analysis yielded a significant and highly robust finding: the optimal solution (450 °C and 120 min) is insensitive to the specific values of w1 and w2. An inspection of our results confirms this. The condition of 450 °C and 120 min coincidentally represents the point of maximum bonding strength (23.56 MPa) and minimum oxide volume (around 12–15 %) within our experimental domain. Because this single condition is the optimum for *both* responses independently, any weighted combination also converges on this same solution.

Finally, the second-order polynomial regression model enables multi-response optimization of bonding strength and oxide volume in diffusion bonding by capturing linear, quadratic, and interaction effects. It shows that temperature negatively impacts bonding strength due to overheating, while the elevated temperatures with long times increase oxide volume due to enhanced oxidation. The interaction effects highlight that temperature and time are not independent, requiring joint optimization. This model supports predictive modeling and process control, enhancing bonding quality and process efficiency.

This model provides a comprehensive understanding of the thermal and diffusion mechanisms, enabling the optimization of bonding conditions for improved joint integrity. This is a powerful result for industrial implementation, particularly for the automotive industry, as it demonstrates a non-conflicting process window where the strongest joint is also the one of highest metallurgical quality, eliminating the need for a complex trade-off.

5. Conclusion

This study provides an in-depth analysis of oxide layer evolution and its influence on the mechanical properties of TLPB in SSM 6063 aluminum alloy using Zamak 2 as a binder follow as:

(1) Demonstrating that bonding temperature at 450, 500 and 550 °C and bonding time at 60 and 120 min critically influence oxide formation and joint integrity. An optimal bonding temperature of 450 °C and 120 min bonding time achieves a superior bond strength at 23.56 MPa.
(2) The elemental composition analysis from EDS data reveals significant variations in oxygen (O), and found that there was high oxide formation at high bonding temperature and bonding time conditions, with bonding temperature at 550 °C showing that oxide volume exceeds 30 % and significantly distributed at the joints leading to poor bonding strength.
(3) The defects found at the joints that cause lower mechanical properties include cracked bond interface, porosity and voids, interfacial separation, and oxide barriers.
(4) The ANOVA results confirm bonding temperature as the most influential factor, followed by bonding time, with a strong interaction. The model explains 89.26 % of total variation (R-Sq), Optimizing bonding temperature is the primary priority, yet bonding time must also be adjusted in tandem for best results. Controllable variables like temperature and time can be regulated, while uncontrollable factors such as oxide layer thickness and microstructural variations introduce process variability. Recognizing both controllable and uncontrollable variables is vital to improving bonding strength and reducing defects in TLPB.

Finally, while this study successfully optimized the TLPB parameters for maximum as-bonded static strength, these findings must be contextualized by considerations for long-term reliability. The brittle nature of the $ZnAl_2$ intermetallic layer, which is fundamental to the bond, presents a potential pathway for fatigue crack initiation. Furthermore, even the optimal joint (at 450 °C) contained a residual oxide. The long-term effect of these oxide remnants as stress concentration points under load is not yet understood.

For industrial applications, such as in the automotive industry, components will experience both long-term aging at elevated temperatures and thermal cycling. The mismatch in thermal expansion coefficients between the SSM 6063 *Al* substrate and the $ZnAl_2$ IMCs could induce thermal fatigue stresses, leading to crack growth. Moreover, prolonged aging could lead to coarsening of the IMC layer or the formation of voids, further degrading joint integrity. Therefore, future work is essential to evaluate the thermal cycling and thermal aging behavior of these joints to validate their long-term reliability.

Beyond these findings, this study offers significant implications for industrial process design, particularly for the automotive industry. The key discovery—that the optimal bond strength (23.56 MPa) occurs at the lowest tested temperature (450 °C) —is a highly non-intuitive and economically favorable result. It challenges the typical 'hotter-is-better' assumption for diffusion, suggesting that this TLPB process can be less energy-intensive and more cost-effective than high-temperature bonding methods.

From a process design perspective, our ANOVA result identifying temperature as the most critical factor sends a clear directive: industrial implementation must prioritize precise thermal control and uniformity, as the data shows overheating leads to a catastrophic loss of strength. Furthermore, our regression model serves as a quantitative process map, enabling engineers to manage the trade-offs between strength, oxide volume, and cycle time. Finally, the acknowledged influence of 'uncontrollable variables' reinforces that a robust and repeatable pre-bonding surface preparation protocol is not just a preliminary step but a critical control point for ensuring industrial-scale reliability.

CRediT authorship contribution statement

D. Maunkhaw: Writing – original draft, Project administration, Investigation, Funding acquisition, Conceptualization. **Y. Dunyakul:** Resources, Formal analysis, Data curation. **C. Meengam:** Writing – review & editing, Visualization, Validation, Supervision, Software, Methodology, Funding acquisition.

Declaration of competing interest

The authors declare that they have no known competing financial interests or personal relationships that could have influenced the work reported in this paper. Furthermore, the authors confirm that the manuscript has been carefully revised in full accordance with the reviewers' comments. All suggestions and critiques raised during the review process have been thoroughly addressed and incorporated into the revised version of the manuscript.

Acknowledgements

The materials for this work were supported by the GISSCO Company Limited and by research grants from the Faculty of Industrial Technology, Songkhla Rajabhat University, and the Faculty of Engineering, Rajamangala University of Technology Srivijaya from Thailand.

Data availability

Data will be made available on request.

References

[1] Y. Li, W. Chunxia, S. Liang, Y. Li, L. Chao, Effect of Al particles addition on microstructure and shear properties of Cu/Sn-1Zn/Cu composite solder joints by transient liquid phase bonding, Mater. Today Commun. 40 (2024) 110129, https://doi.org/10.1016/j.mtcomm.2024.110129.
[2] S. Noh, A. Kimura, Transient liquid phase bonding of ODS ferritic steel with a physical vapor deposited boron thin layer, J. Nucl. Mater. 529 (2020) 151888, https://doi.org/10.1016/j.jnucmat.2019.151888.
[3] J. Carter Stotts, G.B. Thompson, C.R. Weinberger, Modeling the diffusion-controlled phase transformations in transition metal carbide multilayer composites, Results Eng. 18 (2023) 101106, https://doi.org/10.1016/j.rineng.2023.101106.
[4] G. Yan, A. Bhowmik, V. Gill, C.L. Gan, Z. Chen, The study of Ni-Sn transient liquid phase bonded joints under high temperatures, Mater. Charact. 203 (2023) 113099, https://doi.org/10.1016/j.matchar.2023.113099.
[5] M.-H. Heo, Y.-J. Seo, J.-W. Yoon, Transient liquid phase bonding using Cu foam and Cu–Sn paste for high-temperature applications, J. Mater. Res. Technol. 27 (2023) 2856–2867, https://doi.org/10.1016/j.jmrt.2023.10.184.
[6] N.J. Salman, N. Muhayat, T. Hendrato, Effect of complexity design on the physical-mechanical properties of extrusion welded aluminum panel, Results. Eng. 26 (2025) 104906, https://doi.org/10.1016/j.rineng.2025.104906.
[7] J.X. Wang, K.H. Chuang, Y.C. Wu, M.H. Ku, S.W. Ku, M.W. Wu, Mechanical performances of AlN/Al metalized ceramic substrates fabricated by transient liquid phase bonding and pre-oxidation treatment, Ceram. Int. 48 (12) (2022) 16619–16629, https://doi.org/10.1016/j.ceramint.2022.02.206.
[8] D. Zhao, W. Du, Z. Xiu, J. Yan, Ultrasonic-assisted transient liquid phase bonding of SiC ceramic and aluminum alloy using an inactive Zn interlayer, Mater. Charact. 200 (2023) 112902, https://doi.org/10.1016/j.matchar.2023.112902.
[9] Z. Huang, H. Du, L. Liu, Z. Lai, X. Chen, W. Long, W. Wang, G. Zou, Ultrasonic effect mechanism on transient liquid phase bonding joints of SiCp reinforced Mg metal matrix composites using Zn-Al-Zn multi-interlayer, Ultrason. Sonochem. 43 (2018) 101–109, https://doi.org/10.1016/j.ultsonch.2017.11.022.
[10] C. Meengam, Y. Dunyakul, D. Maunkhaw, Joint dissimilar diffusion bonding of SSM-ADC12 Al alloy to SSM 6063 Al alloy, Mater. Today: Proc. (2023) 1–6, https://doi.org/10.1016/j.matpr.2023.05.392.
[11] L. Sun, L. Zhang, C.- Wei, M.- Chen, Y. Zhang, Transient liquid phase bonding (TLPB) of Cu to Cu using Sn interconnect solder reinforced by submicron Al particles, Mater. Today: Proc. 307 (2022) 117686, https://doi.org/10.1016/j.jmatprotec.2022.117686.
[12] C. Liu, A. Liu, Y. Su, Y. Chen, Z. Zhou, C. Liu, Ultrasonically enhanced flux-less bonding with Zn-5Al alloy under ambient condition for high-temperature electronics interconnects, J. Manuf. Process. 73 (2022) 139–148, https://doi.org/10.1016/j.jmapro.2021.10.065.
[13] Q. Jia, Z. Lai, H. Zhang, H. Bai, G. Zou, C. Pan, L. Liu, Mechanism of ultrasonic-assisted transient liquid phase bonding of 6061 Al alloy with cladded Zn-Al alloy in air, J. Mater. Process. Technol. 286 (2020) 116823, https://doi.org/10.1016/j.jmatprotec.2020.116823.
[14] Z. Guo, Z. Li, W. Guo, Y. Guo, J. Li, J. Xiong, Microstructural characteristics and mechanical response of transient liquid-phase diffusion bonding AlCoCrFeNi2.1 high entropy alloy utilizing BNi-5 interlayer, J. Alloys Compd. 1009 (2024) 176904, https://doi.org/10.1016/j.jallcom.2024.176904.
[15] Q. Fang, Z. Guo, L. Zhao, Y. Liu, Microstructure and properties of magnesium alloy joints bonded by using gallium with the assistance of ultrasound at room temperature, Materials. (Basel) 16 (2023) 6994, https://doi.org/10.3390/ma16216994.
[16] W. Reeks, H. Davies, S. Marchisio, A review: interlayer joining of nickel base alloys, J. Adv. Join. Process. 2 (2020) 100030, https://doi.org/10.1016/j.jajp.2020.100030.
[17] R.H. Kadhim, A.O. AL-Roubaiy, H. Omidvar, Transient liquid phase bonding by two-step heating technique of IN939, Jordan J. Mech. Ind. 18 (3) (2024) 621–633, https://doi.org/10.59038/jjmie/180315.
[18] J. Wannasin, S. Janudom, T. Rattanochaikul, R. Canyook, R. Burapa, T. Chucheep, S. Thanabumrungkul, Research and development of gas induced semi-solid process for industrial applications, Trans. Nonferrous Met. Soc. China. 20 (3) (2010) s1010, https://doi.org/10.1016/S1003-6326(10)60622-X. -s1015.
[19] H. Jiang, S. Robertson, S. Liang, Z. Zhou, L. Zhao, C. Liu, Microstructural and mechanical characteristics of Cu-Sn intermetallic compound interconnects formed by TLPB with Cu-Sn nanocomposite, Mater. Today Commun. 33 (2022) 104623, https://doi.org/10.1016/j.mtcomm.2022.104623.
[20] P. Zhao, Z. Li, X. Gao, L. Kuang, Z. Xu, J. Yan, A novel diffusion bonding of 6063Al based on a mode of diffusion-migrating and suspension-broken of surface oxide film, J. Mater. Res. Technol. 27 (2023) 3719–3728, https://doi.org/10.1016/j.jmrt.2023.10.185.
[21] Z. Cai, Y. Li, Y. Xu, J. Chen, X. Li, G. Ma, D. Li, Unified constitutive modeling for hot tensile behavior of TC4 alloy with and without diffusion bonding joint, J. Mater. Res. Technol. 35 (2025) 451–466, https://doi.org/10.1016/j.jmrt.2025.01.014.
[22] C. Meengam, Y. Dunyakul, D. Maunkhaw, S. Chainarong, Transient liquid phase bonding of semi-solid metal 7075 aluminum alloy using ZA27 zinc alloy interlayer, Metals 8 (2018) 0637, https://doi.org/10.3390/met8080637.
[23] A. Baazaoui, S. Msolli, J. Alexis, O. Dalverny, H.S. Kim, Exploring joining techniques for diamond chips on metallized substrates: micro- and nano-scale mechanical testing approach, Next Mater. 7 (2025) 100349, https://doi.org/10.1016/j.nxmate.2024.100349.
[24] J. Cao, M. Zheng, Z. Wang, X. Si, C. Li, X. Wang, Z. He, J. Qi, A low-temperature sealing method for metal-supported oxide fuel cell applications: ni–Sn transient liquid phase bonding, Vacuum. 187 (2021) 110048, https://doi.org/10.1016/j.vacuum.2021.110048.
[25] L.S. Chang, C.F. Huang, Transient liquid phase bonding of alumina to alumina via boron oxide interlayer, Ceram. Int. 30 (8) (2004) 2121–2127, https://doi.org/10.1016/j.ceramint.2003.11.018.
[26] H. Bakhtiari, M. Farvizi, M.R. Rahimipour, A. Malekan, Hot corrosion mechanism in transient liquid phase bonded HX superalloy: effect of bonding time, J. Adv. Join. Process. 11 (2025) 100298, https://doi.org/10.1016/j.jajp.2025.100298.
[27] D.H. Jung, A. Sharma, M. Mayer, J.P. Jung, A review on recent advances in transient liquid phase (TLP) bonding for thermoelectric power module, Rev. Adv. Mater. Sci. 53 (2) (2018) 147–160, https://doi.org/10.1515/rams-2018-0011.
[28] J. Yang, W. Zhao, P. Lin, Q. Zhang, X. Zhang, T. Lin, P. He, Y. Zhuang, An efficient method to engage oxide ceramics in low-temperature interfacial reactions: microstructure evolution and kinetics behaviors based on supercooling in a transient liquid phase bonding joint, J. Mater. Sci. Technol. 151 (2023) 234–244, https://doi.org/10.1016/j.jmst.2022.10.094.
[29] M.H. Heo, Y.J. Seo, J.W. Yoon, Novel and fast transient liquid phase bonding using etched Cu foam/Sn–3.0 Ag–0.5 Cu composite solder preform, Mater. Today Commun. 35 (2023) 105730, https://doi.org/10.1016/j.mtcomm.2023.105730.
[30] G. Yang, X. Li, E. Ren, S. Li, Morphology evolution and grain orientations of intermetallic compounds during the formation of full Cu3Sn joint, Intermetallics. (Barking) 145 (2022) 107555, https://doi.org/10.1016/j.intermet.2022.107555.
[31] C. Imediegwu, S. Graham, D.G. Pahinkar, S. Narumanchi, P. Paret, J. Major, Interdiffusion and formation of intermetallic compounds in high-temperature power electronics substrate joints fabricated by transient liquid phase bonding, Microelectron. Reliab. 137 (2022) 114788, https://doi.org/10.1016/j.microrel.2022.114788.
[32] G.O. Cook, C.D. Sorensen, Overview of transient liquid phase and partial. Transient liquid phase bonding, J. Mater. Sci. 46 (2011) 5305–5323, https://doi.org/10.1007/s10853-011-5561-1.
[33] M.K. Pal, G. Gergely, Z. Gácsi, Growth kinetics and IMCs layer analysis of SAC305 solder with the reinforcement of SiC during the isothermal aging condition, J. Mater. Res. Technol. 24 (2023) 8320–8331, https://doi.org/10.1016/j.jmrt.2023.05.091.
[34] H. Jiang, S. Robertson, S. Liang, Z. Zhou, L. Zhao, C. Liu, Microstructural and mechanical characteristics of Cu-Sn intermetallic compound interconnects formed by TLPB with Cu-Sn nanocomposite, Mater. Today Commun. 33 (2011) 104623, https://doi.org/10.1016/j.mtcomm.2022.104623.
[35] Z. Lang, T. Zou, Z. Ye, T. Wu, W. Wang, J. Yang, J. Huang, Partial transient liquid phase bonding of misoriented single crystal superalloys via a mixture of nickel-chromium-tantalum and nickel-based superalloy powders, J. Mater. Process. Technol. 326 (2024) 118321, https://doi.org/10.1016/j.jmatprotec.2024.118321.
[36] L. Chai, J.H. Huang, J.B. Hou, B. Lang, L. Wang, Effect of holding time on microstructure and properties of transient liquid-phase-bonded joints of a single crystal alloy, J. Mater. Eng. Perform. 24 (2015) 2287–2293, https://doi.org/10.1007/s11665-015-1504-3.
[37] H. Jiang, S. Robertson, S. Liang, Z. Zhou, L. Zhao, C. Liu, Rapid formation of intermetallic joint using Cu-Sn nanocomposite interlayer based on patterned copper nanowire array, Mater. Lett. 307 (2022) 131074, https://doi.org/10.1016/j.matlet.2021.131074.
[38] H. Jiang, S. Robertson, S. Liang, Z. Zhou, L. Zhao, C. Liu, Defect formation and mitigation in Cu/Cu joints formed through transient liquid phase bonding with Cu-Sn nanocomposite interlayer, Microelectron. Reliab. 138 (2022) 114681, https://doi.org/10.1016/j.microrel.2022.114681.

[39] X. Zhang, K.-S. Li, N. Yao, J.-M. Shi, T.-W Lu, W.-R. Nie, R.-Z. Wang, X.-C. Zhang, S.-T. Tu, Transient liquid phase bonding of DD5 single crystal and GH4169 superalloy using BNi-2 interlayer: from microstructural evolutions to mechanical properties, Mater. Sci. Eng. A. 923 (2025) 147723, https://doi.org/10.1016/j.msea.2024.147723.

[40] A.K. Mohammad, S. Morteza, E. Mohammad Hossein, Microstructural and mechanical properties assessment of transient liquid phase bonding of CoCuFeMnNi high entropy alloy, Trans. Nonferrous Met. Soc. China. 31 (10) (2021) 3063–3074, https://doi.org/10.1016/S1003-6326(21)65715-1.

[41] S. HADIBEYK, B. BEIDOKHTI, S.A. SAJJADI, Effect of bonding time and homogenization heat treatment on the microstructure and mechanical properties of the transient liquid phase bonded dissimilar GTD-111/FSX-414 TLP superalloys, J. Alloys. Compd. 731 (2018) 929–993, https://doi.org/10.1016/j.jallcom.2017.10.105.

[42] J. Kangazian, M. Shamanian, Mechanical and microstructural evaluation of SAF 2507 and incoloy 825 dissimilar welds, J. Manuf. Process. 26 (2017) 407–418, https://doi.org/10.1016/j.jmapro.2017.03.006.

[43] T. Li, Y. Lei, L. Chen, H. Ye, X. Liu, X. Li, Advances in mechanism and application of diffusion bonding of titanium alloys, J. Mater. Process. Technol. 337 (2025) 118736, https://doi.org/10.1016/j.jmatprotec.2025.118736.

[44] D. Qu, Z. Zhou, Y. Yum, J. Aktaa, Mechanical characterization and modeling of brazed tungsten and Cu–Cr–Zr alloy using stress relief interlayers, J. Nucl. Mater. 455 (1–3) (2014) 130–133, https://doi.org/10.1016/j.jnucmat.2014.04.026.

[45] Y. Chen, Y. Huang, L. Han, D. Liu, L. Luo, C. Li, C. Liu, Z. Wang, High-strength vacuum diffusion bonding of Cu-plated, sandblasted W and CuCrZr alloy, J. Mater. Res. Technol. 15 (2021) 6260–6271, https://doi.org/10.1016/j.jmrt.2021.11.069.

[46] N. Rajesh Jesudoss Hynes, P. Shenbaga Velu, M. Karthick Raja, D. Jones Joseph Jebaraj, B. Benita, Simulation on graphite to copper joints in nuclear reactor applications by transient liquid phase bonding, Mater. Today: Proc. 47 (19) (2021) 7095–7098, https://doi.org/10.1016/j.matpr.2021.06.209.

[47] M.A. Gharaibeh, Multilayer silver-tin transient liquid phase bonds: constitutive modeling summary, Results Eng. 24 (2024) 103619, https://doi.org/10.1016/j.rineng.2024.103619.

[48] H. Shao, A. Wu, Y. Bao, Y. Zhao, G. Zou, Microstructure characterization and mechanical behavior for Ag3Sn joint produced by foil-based TLP bonding in air atmosphere, Mater. Sci. Eng. A. 680 (2017) 221–231, https://doi.org/10.1016/j.msea.2016.10.092.

[49] M.A. Gharaibeh, Multilayer silver-tin transient liquid phase bonds: constitutive modeling summary, Results Eng. 24 (2024) 103619, https://doi.org/10.1016/j.rineng.2024.103619.

[50] R. Darveaux, Effect of simulation methodology on solder joint crack growth correlation and fatigue life prediction, J. Electron. Packag. 124 (3) (2002) 147–154, https://doi.org/10.1109/ECTC.2000.853299.

[51] M.A. Anas, O.C. Kavian, M. Epstein, Transient liquid phase (TLP) bonding as reaction–controlled diffusion, Mater. Today Commun. 33 (2022) 104293, https://doi.org/10.1016/j.mtcomm.2022.104293.

[52] F.S. Ong, H. Tobe, G. Fujii, E. Sato, Microstructural evolution and mechanical characterization of Nb-interlayer-inserted Ti–6Al–4V/Si3N4 joints brazed with AuNiTi filler, Mater. Sci. Eng. A. 778 (2020) 139093, https://doi.org/10.1016/j.msea.2020.139093.

[53] P. Fitriani, F. Iskandar, P. Colkesen, D.-H. Yoon, Pressureless joining of SiC by molten Si infiltration to the SiC/C filler tape and residual stress analysis, J. Eur. Ceram. Soc. 44 (9) (2024) 5370–5379, https://doi.org/10.1016/j.jeurceramsoc.2023.11.021.

[54] N. Doredla, N. Senthil Kumar, Determination of heat input impact on residual stress, microstructure, and mechanical characteristics of welded ferrite-pearlite (α-P) steel joints by using taguchi optimization approach, J. Adv. Join. Process. 11 (2025) 100278, https://doi.org/10.1016/j.jajp.2024.100278.